***Title:*** The cell wall regulates dynamics and size of plasma-membrane nanodomains in *Arabidopsis*.

***One sentence summary:*** Size and mobility of protein nanodomains in the plant plasma-membrane are regulated by interaction with the cell wall extracellular matrix.

***Authors:*** McKenna JF[1], Rolfe DJ[2], Webb SED[2,3], Tolmie AF[1], Botchway SW[2], Martin-Fernandez ML[2], Hawes C[1] & Runions J[1].

***Affiliations:*** 1. Department of Biological and Medical Sciences, Oxford Brookes University, Sinclair Annex, Gipsy Lane, OX3 0BP
2. Central Laser Facility, Research Complex at Harwell, Science and Technology Facilities Council, Rutherford Appleton Laboratory, Oxfordshire OX11 0QX, United Kingdom
3. Present address: BBSRC (UKRI), Polaris House, N Star Ave, Swindon, SN2 1UH, United Kingdom

***Abstract:*** Plant plasma-membrane (PM) proteins are involved in several vital processes, such as detection of pathogens, transportation and cellular signalling. Recent models suggest that for these proteins to function effectively there needs to be structure within the PM allowing, for example, proteins in the same signalling cascade to be spatially organised. Here we demonstrate that several proteins with divergent functions are located in clusters of differing size in the membrane when imaged using sub-diffraction-limited Airyscan confocal microscopy. In addition, single particle tracking reveals that these proteins move at different rates within the membrane. We show that the actin and microtubule cytoskeletons appear to significantly regulate the mobility of one of these proteins (the pathogen receptor FLS2) within the plasma-membrane. We further demonstrate that the cell wall is critical for the regulation of cluster size by affecting single particle dynamics of two proteins with key roles in morphogenesis (PIN3) and pathogen perception (FLS2). We propose a model in which the cell wall and cytoskeleton are pivotal for differentially regulating protein cluster size and dynamics thereby contributing to the formation and functionality of membrane nanodomains.

***Main text:***

## ***Introduction***

The plasma membrane (PM) plays key roles in compartmentalisation and protection of cells from the environment (1). In plants, proteins located within the PM are critical for signal perception, transduction and the controlled import and export of molecules (2). The structure

of the PM was described by the fluid mosaic-model as a diffuse mixture of proteins in motion (3). However, this does not fit observations of protein spatial heterogeneity in membranes and subsequent models have been developed (4) which incorporate so-called lipid rafts, detergent resistant membranes, cytoskeleton corralling and extracellular matrices as mechanisms of spatial constraint (5).

While proposed models of PM organisation are under dispute and no single model explains all experimental observations across different model organisms, a number of proteins are known to locate to specific domains in the plant PM. The best studied of these in plants is the REMORIN family (6–8). Members of the REMORIN family form non-overlapping PM nanodomains (6). We define nanodomains here as others have previously: distinguishable submicron protein or lipid assemblies which are 20nm to 1µm in size (8). While the patterning of these REMORIN nanodomains has been well described, no known functional role has thus far been ascribed to them. Proteins critical for normal morphogenesis and development such as PIN1 and PIN2 are localized to defined domains in the PM. PIN2 has been shown, using STED super-resolution imaging, to form clusters in the PM, with controlled endo-, and exocytosis from adjacent membrane regions to the localization domain (9). Additionally, the pathogen receptor FLS2 has been shown to localise to nanodomains in the plasma-membrane (10). Spatial organisation of proteins in the PM is, therefore, important for development and response to the environment, but how is membrane domain patterning regulated?

The underlying cytoskeleton and outlying cell wall can be thought of as a continuum with the PM (2, 11). There are numerous examples of cytoskeletal and PM mechanisms which play roles in cell wall production and regulation of cell wall patterning: i) the microtubule-guided CesA complex determines patterns of cellulose microfibril deposition (12, 13), ii) microtubule-associated MIDD1 is involved in secondary cell-wall pit formation (14), iii) the CASP family of proteins form a PM nanodomain which defines the site of Casparian strip formation (15), and iv) FORMIN1 is anchored within the cell wall, spans the PM and nucleates actin filaments as part of a mechanism in which cell-wall anchoring is required for actin cytoskeleton organisation (16). The cell wall has been shown to have a role in regulating the lateral diffusion of two ‘minimal’ membrane proteins which have GFP projecting into the cell wall space (5). ‘Minimal’ membrane proteins are artificially-created peptides which localise to the plasma membrane via one of a number of association mechanisms. They were designed as fluorescent protein fusions and have no predicted protein interactions or biological functions. The plant cell wall is also required for normal localisation of PIN2 in the membrane and hence regulation of cell polarity (17). These examples highlight the possibility that the components of the cytoskeleton / PM / cell wall

continuum can regulate each other, with cell-wall regulation of plasma-membrane, and cytoskeleton organization already observed (5, 18).

A systematic study of a number of PM proteins in transiently and stably expressing plant cells has demonstrated a difference in their lateral mobility (5). This was achieved by Fluorescence Recovery After Photobleaching (FRAP) using high temporal but low spatial resolution. With the ever increasing toolkit of sub-diffraction limited microscopy techniques developed over recent years we used Airyscan imaging (19, 20) of flat membrane sheets in stably expressing *A. thaliana* hypocotyl cells to image PM structure with high spatial resolution. We chose to use Airyscan imaging and Total Internal Reflection Fluorescence - Single particle (TIRF-SP) imaging as they do not involve the use of special fluorophores required for PALM or a high power depletion laser used in STED which causes damage of aerial tissue in plants due to the presence of light absorbing chloroplasts. A combination of TIRF-SP and Airyscan imaging allows fast temporal acquisition with sub-diffraction limit resolution (down to 140 nm for the latter) in all plant tissues with the use of any existing fluorophore (19).

We show that FLS2, PIN3, BRI1 and PIP2A, form clusters of differing size from 164 to 231 nm. Upon further investigation actin and microtubule cytoskeletons regulate the diffusion rate of the pathogen receptor FLS2 but not the hormone transporter PIN3. Furthermore, cluster size and diffusion rate of both FLS2 and PIN3 are regulated by cellulose and pectin components of the cell wall.

We hypothesise that the constraint of the cell wall on PM proteins and differential regulation by the actin and microtubule cytoskeletons can contribute to PM organisation by altering protein dynamics and hence nanodomain size. This is a mechanism by which proteins can exist within different sized nanodomains.

## Results

### ***Plasma-membrane proteins form clusters within the membrane***

We chose several well characterised PM proteins which have a variety of functions in order to determine how different proteins are organized in the PM and whether their dynamic behaviour differs. Airyscan imaging and determination of nanodomain full width half maximum (FWHM) demonstrated that proteins form clusters within the PM which are not resolved by diffraction-limited confocal imaging (Fig.1. & S1). Protein clusters were observed and measured for the auxin transporter PIN3 (Puncta FWHM, = 166.7±31.1 nm, Fig.1), the pathogen receptor FLS2 (Puncta FWHM = 164.3±32.0 nm, Fig.1), the hormone receptor BRI1 (Puncta FWHM = 172.6±41.3 nm, Fig.S1) and the aquaporin PIP2A (Puncta FWHM =

194.3±66.8 nm, Fig.S1). Cluster diameter was determined by full width half maximum (FWHM) measurements of line profiles over randomly selected nanodomains. Each protein observed had a nanodomain diameter under the 250nm abbe resolution limit of confocal microscopy using GFP (Fig.1D)(21). When compared to REM1.3 (Puncta FWHM = 231.0±44.8 nm, Fig.1) which is known to form highly stable nanodomains resolvable by confocal microscopy within the PM (6), FLS2 and PIN3 clusters are significantly smaller and are more dynamic within the membrane (Fig.1C and S1).

***<u>Proteins move at different speeds within the membrane</u>***

In order to determine the diffusion rate of select proteins within the PM we used Total Internal Reflection Fluorescence - Single Particle (TIRF-SP) imaging which yields high spatial and temporal resolution tracking information. We chose to focus on the PM proteins p35S::paGFP-LTI6b, p35S::PIP2A-paGFP, pFLS2::FLS2-GFP and pPIN3::PIN3-GFP as these cover a diverse range of functions from pathogen perception, to morphogen transport and resource acquisition (Fig.2, Supplemental movie 1). It is worth noting, TIRF-SP imaging and tracking can be performed with both photoactivatable GFP (paGFP) and GFP and with overexpression or native promoters. However, expression needs to be within a range sufficient for signal detection but not so bright as to saturate the detector. This was the case for expression driven by the PIN3 and FLS2 promoters in the *A. thaliana* hypocotyl. Here we show diffusion rates from fitting a constrained diffusion model to the initial 4 seconds of particle tracking (Fig.2A-D). As has previously been shown by FRAP (5), the marker protein paGFP-LTI6b displays a significantly greater diffusion rate ($D=0.063\pm0.003\mu m^2/s$, $p<0.01$, Fig.2C & S2) when compared to the other proteins. The aquaporin PIP2A-paGFP ($D=0.026\pm0.004\mu m^2/s$) displays an enhanced diffusion rate when compared to FLS2-GFP ($D=0.005\pm0.004\mu m^2/s$, $p<0.01$) and PIN3-GFP ($0.012\pm0.001\mu m^2/sec$, $p<0.01$, Fig.2C). FLS2-GFP and PIN3-GFP showed statistically different diffusion ($p\leq0.05$). Fitting a pure diffusion model to the first two points of each curve shows the same pattern for protein diffusion rates, showing that our conclusions are robust to the choice of model although the precise diffusion values are different (Fig.2&S2). However, unlike the constrained diffusion rate for the proteins investigated, the constrained area occupied by the particle was shown to be the same for PIP2A-paGFP, FLS2-GFP and PIN3-GFP, with only paGFP-LTI6b showing a statistically significant increase in constrained area size compared to the other proteins ($p<0.05$-$0.01$, Fig.2D). Thus, we have demonstrated by single particle imaging that PM proteins move at different speeds within the membrane even when the areas that they move within are relatively similar in size.

***The actin and microtubule cytoskeletons differentially regulate PM protein dynamics***

The cell surface exists as a continuum containing the cell wall, PM and cytoskeleton (11). Previously it had been shown by FRAP that incubation of seedlings with cytochalasin D or oryzalin which depolymerize actin microfilaments or microtubules, respectively, did not affect the dynamics of 'minimal' membrane proteins (5). Here, upon actin or microtubule depolymerisation, no changes were observed in the constrained diffusion rate for PIN3-GFP and paGFP-LTI6b (Fig 3A&E, Supplemental movie 2). Interestingly, both showed a statistically significant increase in constrained area after actin depolymerisation ($p<0.05$, Fig 3B&F). Conversely, upon actin or microtubule depolymerisation, FLS2-GFP displayed an increase in protein diffusion rate, (Mock; D = 0.0053 ± 0.0004$\mu m^2$/s, Lat-B; D = 0.011 ± 0.002$\mu m^2$/s, Oryzalin; D = 0.013 ± 0.002 $\mu m^2$/s, $p<0.001$, Fig 3C, Supplemental movie 2) but not in constrained area (Fig. 3D). This was also observed for instantaneous diffusion rates (Fig.S3). Therefore, the actin and microtubule cytoskeletons can differentially regulate the mobility of proteins in the membrane.

***The cell wall regulates PM diffusion rate, constrained area and nanocluster size***

Lateral diffusion denotes protein dynamics within the plane of a membrane. Previously it was shown using a combination of plasmolysis and protoplasting treatments that, upon removal of the cell wall constraint, protein lateral diffusion of 'minimal' PM proteins with extracellular GFP is increased (5). Therefore, we hypothesized that the cell wall constrains the lateral diffusion rate of biologically functional proteins within the membrane. Here, we performed TIRF-SP imaging of paGFP-LTI6b, PIN3-GFP and FLS2-GFP in combination with pharmacological perturbation of the cell wall (Fig.4-5). We decided to use two biologically active proteins with divergent function under control of their own promoters. The cellulose synthase specific herbicide DCB (22) and the pectin demethylesterase EGCG (23) were used to impair either cellulose synthesis or pectin status (Fig.4-5) and hence the cell wall. Upon cell wall impairment with either, there was a non-significant trend towards increased constrained diffusion rate (Fig. 4B) and constrained area (Fig. 4C) for paGFP-LTI6b (Fig.4, Supplemental video 3). Therefore, over one hour of treatment with either drug, an alteration in cell wall structure did not dramatically alter paGFP-LTI6b dynamics within the membrane. There was however a statistically significant increase in the instantaneous diffusion rate of paGFP-LTI6b upon cellulose or pectin perturbation of the cell wall (Fig.S5A&B, Mock; instantaneous D = 0.066 ± 0.005$\mu m^2$/s, DCB; instantaneous D = 0.085 ± 0.004$\mu m^2$/s, EGCG; instantaneous D = 0.085 ± 0.003 $\mu m^2$/s). In addition, upon plasmolysis with either NaCl or mannitol, the paGFP-LTI6b diffusion rate was significantly increased in

the PM (Fig.S4A-E, Supplemental video 4). Therefore, minor cell wall perturbation by impairing individual components does not affect the constrained diffusion rate of paGFP-LTI6b, but significant separation of the cell wall from the cell cortex and PM by plasmolysis does.

We also performed TIRF-SP imaging of the PM proteins PIN3-GFP and FLS2-GFP after cell wall perturbation (Fig. 5, supplemental movie 5). We chose PIN3-GFP and FLS2-GFP as their diffusion rates in untreated cells were reduced compared to paGFP-LTI6b and PIP2A-paGFP (Fig.2). In addition, PIN3 is functionally active in the hypocotyl as the flow of auxin is constant throughout plant development. Conversely, FLS2 should not be signalling in the absence of its ligand flg22 (24). In this study we tracked both active and non-active biologically functioning proteins and any similarities observed should demonstrate overall effects of the cell wall on PM protein dynamics. Unlike paGFP-LTI6b, both PIN3-GFP and FLS2-GFP showed significantly increased constrained diffusion rate and area upon treatment with either DCB or EGCG (Fig 5A-H). FLS2 diffusion was 0.0054 ± 0.0004$\mu m^2$/s, DCB; 0.0091 ± 0.001$\mu m^2$/s, EGCG; 0.013 ± 0.001$\mu m^2$/s, $p<0.001$. PIN3 diffusion was 0.012 ± 0.001$\mu m^2$/s in control, 0.0159 ± 0.0008$\mu m^2$/s in DCB and 0.018 ± 0.001$\mu m^2$/s in EGCG ($p<0.05$). Therefore, perturbation of either cellulose or pectin components of the cell wall results in these proteins diffusing faster and over a larger area (Fig 5). Furthermore, as a control, plasmolysis with either NaCl or mannitol and subsequent separation of the cell wall and PM caused an increase in diffusion rate and constrained area of both (Fig.S4F-O, Supplemental movie 6), with the exception of the constrained region for FLS2-GFP (Fig.S4J).

In combination with the TIRF-SPT, Airyscan imaging of PIN3-GFP and FLS2-GFP demonstrates that nanodomain size significantly increases upon perturbation of either cellulose synthesis or pectin status (Fig 5D&H). FLS2-GFP control nanodomain size was 161.4nm ± 41.5 SD, DCB 180.7nm ± 65.35 SD and EGCG 182.1nm ± 61.94 SD (Fig. 5D). Changes in nanodomain size after DCB and EGCG were statistically significant compared with mock treatment ($p\leq0.0001$, ANOVA), however there was no statistically significant difference between FLS2-GFP DCB and EGCG treated nanodomain size ($p\geq0.05$, ANOVA). PIN3 control nanodomain size was 173.1nm ± 70.1 SD, DCB was 187.6nm ± 72.29 SD and EGCG was 191.5nm ± 50.92 SD (Fig. 5H). As with FLS2-GFP, PIN3-GFP nanodomain FWHM were statistically significant between control and DCB or EGCG ($p\leq0.0001$, ANOVA), however there was no statistical significance between DCB and EGCG ($p\geq0.05$, ANOVA).

Therefore, for FLS2-GFP and PIN3-GFP upon either plasmolysis, or cellulose and pectin disruption, there is an increase in constrained diffusion rate, constrained area, and nanodomain size. This demonstrates that the cell wall has a direct role in regulating both PIN3-GFP and FLS2-GFP protein dynamics and nanodomain size in the membrane.

## ***Discussion***

### ***Proteins reside in different sized nanodomains and display different dynamics in the plasma membrane***

Here we have shown that several proteins form nanodomains within the plasma membrane which can be resolved with sub diffraction-limited imaging. Furthermore, the proteins we chose to image have diverse biological functions and have not been shown to have domains anchored into the cell wall, such as FORMIN1(16), AGP4 (5) or WAK1&2 (25). The auxin efflux protein PIN2 has been shown to form nanodomains in the membrane using STED microscopy of between 100-200nm which is the same observed by us for PIN3 using Airyscan imaging (Fig. 1 and (9). however in the same investigation BRI1 was found to have weak protein heterogeneity (9), which is in contradiction to our findings (Fig.S1) and those of others (26). This was however in roots and we imaged in hypocotyls so this could be explained by tissue specific differences such as the cell wall, which we and others have shown to be important for nanodomain size (Fig 5 and (5). We have shown that nanodomain size is significantly different for the various proteins investigated, with all proteins showing statistically significant differences in nanodomain size (Figs. 1&S1). Recent work has demonstrated that both FLS2 and BRI1 form nanodomains in the membrane (10, 26–28), which supports our study. However, the reported size for BRI1-GFP and FLS2-GFP nandomains is significantly larger than we observe here (10). This could be due to the imaging mode used and the image analysis methods employed.

Using TIRF single particle (TIRF-SP) imaging and tracking, we have demonstrated that FLS2 and PIN3 have different diffusion rates within the plane of the PM. Furthermore, the dynamics of the proteins investigated are complex and not uniform. As shown previously, the paGFP-LTI6b diffusion rate is high relative to most other proteins thus far investigated (5). However it only has two residues projecting into the extracellular space compared to FLS2-GFP and PIN3-GFP which have larger extracellular domains (29, 30). ‘Minimal’ membrane proteins which are PM anchored and have an intracellular GFP tag have faster diffusion rates than ‘minimal’ membrane proteins which have extracellular GFP (2, 5).Therefore, with regards to investigation of PM protein dynamics, the study of functional biologically relevant proteins which contain extracellular domains is more instructive than marker proteins such as paGFP-LTI6b although the dynamics of biologically functional PM localised proteins which have no extracellular domains still needs to be investigated.

To conclude, protein domain diffusion rate heterogeneity exists in the plant PM for all the proteins investigated in this study. This is similar to observations using dSTORM super

resolution imaging of individual TCR molecules in activated human T cells (31) and proteins located in membrane sheets imaged with STED (32). Therefore, heterogeneity of membrane protein diffusion rates is a common theme across kingdoms. It is interesting to note that all proteins imaged also form differently sized nanodomains within the PM. Heterogeneity of protein domain size and diffusion rate suggests that nanodomains of PM localised proteins must show substantial crowding / overlap within the membrane. However, we have only imaged one labelled nanodomain at a time in this study. It will be interesting to extend this work to investigate protein species heterogeneity within the imaged nanodomains. Protein association within nanodomains would convey rapid functionality in multi-protein response pathways. Additionally, it could account for how signalling pathways which rely on common components such as FLS2 and BRI1 can lead to environmental or development responses as has been shown previously(10). This could also account for cross talk between different pathways when components are localised to specific but partially overlapping nanodomains.

***<u>The actin and microtubule cytoskeleton can regulate the diffusion of FLS2 but not PIN3 and LTI6b.</u>***

We have demonstrated that the actin and microtubule cytoskeletons do not uniformly regulate the dynamics of PM proteins. The actin and microtubule cytoskeletons only regulate the constrained diffusion rate of FLS2, which has increased lateral dynamics after depolymerization of either network (Fig. 3C). Both PIN3-GFP and paGFP-LIT6b showed no statistical difference in diffusion rate upon cytoskeleton depolymerization, but did show an increase in the constrained area size when viewed as single particles (Fig. 3A-B & E-F). However, the constrained area was not altered for FLS2 by cytoskeleton depolymerization (Fig. 3). PIP2A has been shown by sptPALM imaging to have an increased diffusion rate upon depolymerization of the actin cytoskeleton (33), but, no difference was reported for PIP2A upon Oryzalin treatment to depolymerize the microtubule cytoskeleton. The actin and microtubule cytoskeleton regulation of some PM localised proteins is further demonstrated by a recent report showing that the pathogen perception signalling protein BIK1 has been shown to co-localise to microtubules but not the actin cytoskeleton (10). In addition, actin and microtubule depolymerisation resulted in loss of and enlargement of nanodomain structure of REM1.2-YFP respectively (34). Differential regulation of proteins by the cytoskeleton would contribute to proteins forming differently sized nanodomains and having differing diffusion rates in the membrane, which we have observed. All proteins investigated in this study show differently sized nanodomains with different dynamics in the membrane (Fig. 1 & S1). The regulation of PM proteins by the cortical actin cytoskeleton has been investigated widely in mammalian cell systems and modelling has demonstrated that the

actin cytoskeleton is sufficient to regulate heterogeneities in PM protein organisation (35). This could partly account for the differences we observe in PM nanodomains size and dynamics *in planta.*

***<u>The cell wall regulates PM nanodomain size and dynamics</u>***

To determine any effect that perturbations in different cell wall matrix components might have on the diffusion rate of proteins within the PM we perturbed cellulose synthesis and pectin methylation status. Neither of these treatments had a statistically significant effect on the constrained diffusion rate or area of LTI6b in the membrane (Fig. 3). paGFP-LTI6b is an extremely mobile protein and shows very different characteristics during TIRF-SP tracking to the other biologically functioning PM proteins investigated. We hypothesize that due to the relatively fast diffusion rate of the protein in the PM and only having two residues in the apoplast, it is under relatively little constraint from the cell wall and hence, a minor cell wall perturbation over a short period such as those performed here with DCB and EGCG would not dramatically alter its diffusion rate. However, a major separation of the cell wall and PM during plasmolysis did significantly increase its diffusion rate in the membrane (Fig. S4).

PIN3 and FLS2 showed rapid changes in both constrained diffusion rate and constrained area upon cellulose or pectin disruption (Fig.5). Therefore the cell wall acts to constrain the lateral mobility of these proteins within the PM. We have demonstrated that cell wall structure also regulates nanodomain size (Fig. 5D&H). This is surprising as after cell wall perturbation for 20 minutes the cellulose synthase complexes are removed from the PM (13) but no other changes have been reported until much later with transcriptional changes, phytohormone induction and lignin deposition occurring at 4-7 hours of treatment (36). Therefore, minor cell wall perturbations rapidly affect PM nanodomain structure and dynamics. That such a short treatment has a profound effect on PM protein dynamics demonstrates how intimately related the cell wall and PM are. This could be an as yet undescribed mechanism of the plant cell that allows it to rapidly respond to mechanical stimuli. In addition, it is interesting that separating the cell wall and PM that occurs during plasmolysis results in increased diffusion of paGFP-LTI6b, whereas specifically impairing a single component over a short time frame did not. This could be because the cell wall has a global effect on the dynamics of all proteins with the severity depending on the size of any extracellular domains or residues. In addition, a subset of proteins with extracellular residues such as PIN3-GFP and FLS2-GFP might chemically interact with cell wall domains as has been demonstrated for Formin1 (5), and breakage of these chemical bonds resulting from plasmolysis might destabilize the entire membrane structure. The dense extracellular matrix

of brain synapses has been shown to regulate the lateral mobility of AMSP-type glutamate receptors (37). Therefore, the role of extracellular matrices in governing the dynamics of PM proteins is common across kingdoms.

It would be interesting to determine if changes in nanodomain size affect the signalling functions of either PIN3 or FLS2 and subsequent hormone transport or ligand binding. Here we show using native promoter expression of tagged proteins that their dynamics and nanodomain size are regulated by the cell wall. The pathogen receptor protein FLS2 has lowered lateral mobility when treated with flg22 in protoplasts (38). Recently, it has been shown that flg22 treatment results in decreased dynamics of FLS2 nanodomains (10), confirming the FRAP result reported previously (38). This has been demonstrated for the aquaporin PIP2A which, upon salt stress, co-localizes with the membrane nanodomain marker FLOT1 and shows changes in its mobility within the membrane (39). In addition, membrane nanodomains have been shown to be important for the activation of receptor-mediated signalling upon ligand perception and subsequent clathrin-mediated endocytosis (26). Therefore, given the cell wall plays a role in regulating the size of these nanodomains and their dynamics, cell wall regulation of PM nanodomains is of fundamental importance to signalling *in planta*

To conclude, we have shown that a number of PM proteins form nanodomains within the PM and that these are of sufficient size for imaging using sub-diffraction limited techniques such as the Zeiss Airyscan system. These nanodomains are of different sizes and their dynamics and size can be differentially regulated by the actin and microtubule cytoskeletons and the cell wall. As yet, very limited information exists as to how PM proteins form nanodomains. We demonstrate here that the cell wall plays a key role in regulation of protein nanodomain size and lateral mobility for the pathogen receptor FLS2 and the auxin transporter PIN3. We hypothesize that the cytoskeleton and cell wall slow nanodomain dynamics sufficiently to allow relatively static distribution of functional proteins so that they are well placed spatially for optimum association.

## ***Materials and Methods***

### ***Plant material***

The seed lines used have been previously described; p35S::paGFP-LTI6b (5), pFLS2::FLS2-GFP (24), pPIN3::PIN3-GFP , p35S::PIP2A-GFP (40), p35S::PIP2A-paGFP (41), pUBQ10::REM1.3-YFP (6) and pBRI1::BRI1-GFP (42). *A. thaliana* seeds were sterilised in 70% ethanol for 5 minutes, 50% bleach for 5 minutes and washed four times with water. Seeds were placed on square agar plates composed of ½ strength MS with MES and 0.8% Phytagel. Seedlings were then stratified on plates for 2 days at 4 in the dark.

Plates were then placed in a growth chamber set to 16:8 long day, 23℃ 120µ Einstein's for 5 days before imaging.

***Chemical treatments***

*A. thaliana* seedlings were treated in 8ml $dH_2O$ 6 well plates for 1 hour with the following concentrations, all made from 1000X stocks; 5µM DCB, 50µM EGCG, 0.5M mannitol, 100mM NaCl, 2.5µM Latrunculin-B and 10µM Oryzalin. DCB, isoxaben, Latrunculin-B and Oryzalin were dissolved in DMSO and EGCG was dissolved in ethanol.

***Confocal and Airyscan microscopy***

Seedlings were imaged after five days of growth by mounting them on microscope slides and no1.5 coverslips immersed in $dH_2O$. Slides and coverslips were held down with micropore tape. A Zeiss LSM880 equipped with an Airyscan detector was used for improved confocal microscopy. Airyscan imaging was performed using 488 and 514nm lasers for GFP and YFP respectively were used at 1% transmission with a dual 495-550 band pass and 570nm long pass filter. For standard confocal imaging the same emission wavelength was imaged with a GaAsP detector. To avoid chlorophyll autofluorescence a 615nm shortpass filter was used. The 100x/1.46 DIC M27 Elyra oil immersion lens was used for all imaging. A 5X zoom was used to image flat membrane sheets and imaging conditions were all set according to Zeiss optimal Airyscan framesize (for 5X zoom, 404x404). Frame sizes were kept the same for standard confocal imaging. For single particle experiments, N= a minimum of 12 cells imaged across 3 biological replicates per condition, the number of single particles tracked per condition is displayed in Table S1. For all Airyscan data N = ≤64 punctae measured per cell for 36 cells across three biological repeats, exact numbers for each condition can be seen in Table S2.

***Airyscan image analysis***

PM protein nanodomain size was determined by imaging using the above conditions. Using FIJI an 8X8 grid was placed over the image and line profiles determined for the brightest nanodomain in each grid cell. The full width half maximum of these line profiles was then determined and this data was collated in Graphpad Prism version 7. Scatter dot plots were produced with error bars denoting the standard deviation. The statistical tests performed was an ANOVA with multiple comparisons. Kymographs were produced from 55 subsequent images comprising 8 seconds of imaging the PM. Multiline kymograph in FIJI was used to produce a kymograph with the line originating in the bottom left corner at a 45 degree angle to the top right for each data-set.

***TIRF-SP Imaging***

TIRF imaging was performed as described in (5) using an inverted microscope (Axio Observer, Zeiss) equipped with a 100X objective (α-Plan-Apochromat, NA = 1.46; Zeiss)

and TIRF slider (Zeiss), 488-nm laser excitation (Stradus Versalase, Vortran), HQ525/50-nm emission filter (Chroma), and an electron-multiplication CCD (iXon+; Andor). The exposure time was 50 ms.

***<u>TIRF-SP tracking</u>***

From single particle tracks, mean squared displacement (MSD) curves were calculated as MSD($\Delta T$)=<|$\mathbf{r}_i(T+\Delta T)$-$\mathbf{r}_i(T)$|$^2$> where |$\mathbf{r}_i(T+\Delta T)$-$\mathbf{r}_i(T)$| is the displacement between position of track *i* at time *T* and time *T*+$\Delta T$ and the average is over all pairs of points separated by $\Delta T$ in each track. The errors in the MSD curve were calculated by repeating the MSD curve calculation 200 times, each time on a different synthetic dataset created by randomly resampling with replacement the tracks present within each dataset, and the datasets present (bootstrap resampling (43)). The distribution of MSDboot$_j$($\Delta T$) curves about the MSD curve for the unresampled data, MSD($\Delta T$), should be close to the distribution of MSD($\Delta T$) about the true MSD curve (43). Therefore a posterior sample of 200 MSD curves MSDpost$_j$($\Delta T$) can be calculated from these 200 bootstrap MSD curves MSDboot$_j$($\Delta T$) (*j*=1..200).

$$MSD(\Delta T) - MSDpost_j(\Delta T) = MSDboot_j(\Delta T) - MSD(\Delta T)$$

so

$$MSDpost_j(\Delta T) = 2MSD(\Delta T) - MSDboot_j(\Delta T)$$

Subsequent model fits (see below) were performed on each posterior MSD curve sample to naturally yield joint posterior samples of the fitted model parameters suitable for determining confidence intervals, error bars and statistical tests. A$\chi^2$fit was performed for each posterior sample using the standard deviation of the posterior MSDs at each $\Delta T$ as the error estimate for calculating $\chi^2$.

The models fitted were free diffusion with parameters diffusion rate *D* and localisation error $\sigma_{loc}$, which was fitted to the first two points on the curve, for which

$$MSD(\Delta T) = 4D\Delta T + 4\sigma_{loc}^2 \quad (44)$$

and constrained diffusion with parameters initial diffusion rate *D*, confinement region size *L* and localisation error $\sigma_{loc}$ where

$$MSD(\Delta T) = \frac{L^2}{3}\left[1 - exp\left(\frac{-12D\Delta T}{L^2}\right)\right] + 4\sigma_{loc}^2 \quad (44)$$

The confidence intervals for each parameter were chosen as the midpoint ± half width of shortest interval containing 69% of the posterior probability for that parameter.

We assume that for the null hypothesis that posterior samples 1 and 2 correspond to the same value of quantity $x$, the probability of a given difference $\Delta x$ is the same as the measured probability of $\Delta x$ about its mean, i.e.

$$P(\Delta x|NULL) = P(\Delta x - \langle\Delta x\rangle|sample1, sample2)$$

The probability that $|\Delta x|$ is at least $\langle\Delta x\rangle$ given the null hypothesis is then

$$P(|\Delta x| > |\langle\Delta x\rangle||NULL) = \int_{|\langle\Delta x\rangle|}^{\infty} P\left(|\Delta x - \langle\Delta x\rangle||sample1, sample2\right)$$

We use this as a non-parametric P-value for the null hypothesis that the two posterior samples measure the same value. In the case of normally distributed posteriors from normally distributed sample measurements this gives the same P-values as the 2-sided Welch's t-test.

***<u>References:</u>***


1. Bernardino de la Serna J, Schütz GJ, Eggeling C, Cebecauer M (2016) There Is No Simple Model of the Plasma Membrane Organization. *Front Cell Dev Biol* 4(September):1–17.
2. Martinière A, Runions J (2013) Protein diffusion in plant cell plasma membranes: the cell-wall corral. *Front Plant Sci* 4(December):515.
3. Singer SJJ, Nicolson GLL (1972) The fluid mosaic model of the structure of cell membranes. *Science (80- )* 175(4023):720–731.
4. Malinsky J, Opekarová M, Grossmann G, Tanner W (2013) Membrane microdomains, rafts, and detergent-resistant membranes in plants and fungi. *Annu Rev Plant Biol* 64:501–29.
5. Martinière A, et al. (2012) Cell wall constrains lateral diffusion of plant plasma-membrane proteins. *Proc Natl Acad Sci U S A* 109(31):12805–10.
6. Jarsch IK, et al. (2014) Plasma Membranes Are Subcompartmentalized into a Plethora of Coexisting and Diverse Microdomains in Arabidopsis and Nicotiana benthamiana. *Plant Cell* 26(4):1698–1711.

7. Leborgne-castel N, et al. (2009) Remorin , a Solanaceae Protein Resident in Membrane Rafts and Plasmodesmata , Impairs Potato virus X Movement. 21(May):1541–1555.
8. Ott T (2017) Membrane nanodomains and microdomains in plant–microbe interactions. *Curr Opin Plant Biol* 40:82–88.
9. Kleine-Vehn J, et al. (2011) Recycling, clustering, and endocytosis jointly maintain PIN auxin carrier polarity at the plasma membrane. *Mol Syst Biol* 7(540):540.
10. Bücherl CA, et al. (2017) Plant immune and growth receptors share common signalling components but localise to distinct plasma membrane nanodomains. *Elife* 6:1–28.
11. McKenna JF, Tolmie  a F, Runions J (2014) Across the great divide: the plant cell surface continuum. *Curr Opin Plant Biol* 22:132–140.
12. Bubb MR, Spector I, Beyer BB, Fosen KM (2000) Effects of jasplakinolide on the kinetics of actin polymerization. An explanation for certain in vivo observations. *J Biol Chem* 275(7):5163–5170.
13. Paredez AR, Somerville CR, Ehrhardt DW (2006) Visualization of cellulose synthase demonstrates functional association with microtubules. *Science* 312(5779):1491–5.
14. Oda Y, Fukuda H (2012) Initiation of cell wall pattern by a Rho- and microtubule-driven symmetry breaking. *Science* 337(6100):1333–6.
15. Roppolo D, et al. (2011) A novel protein family mediates Casparian strip formation in the endodermis. *Nature* 473(7347):380–3.
16. Martinière A, Gayral P, Hawes C, Runions J (2011) Building bridges: formin1 of Arabidopsis forms a connection between the cell wall and the actin cytoskeleton. *Plant J* 66(2):354–65.
17. Feraru E, et al. (2011) PIN polarity maintenance by the cell wall in Arabidopsis. *Curr Biol* 21(4):338–43.
18. Tolmie F, et al. (2017) The cell wall of Arabidopsis thaliana influences actin network dynamics. *J Exp Bot* 68(16):4517–4527.
19. Huff J (2015) The Airyscan detector from ZEISS: confocal imaging with improved signal-to-noise ratio and super-resolution. *Nat Methods* 12(12):i–ii.
20. Korobchevskaya K, Lagerholm B, Colin-York H, Fritzsche M (2017) Exploring the Potential of Airyscan Microscopy for Live Cell Imaging. *Photonics* 4(3):41.
21. Schermelleh L, Heintzmann R, Leonhardt H (2010) A guide to super-resolution fluorescence microscopy. *J Cell Biol* 190(2):165–75.
22. Peng L, Zhang L, Cheng X, Fan L-S, Hao H-Q (2013) Disruption of cellulose synthesis by 2,6-dichlorobenzonitrile affects the structure of the cytoskeleton and cell wall construction in Arabidopsis. *Plant Biol (Stuttg)* 15(2):405–14.

23. Wolf S, Mravec J, Greiner S, Mouille G, Höfte H (2012) Plant cell wall homeostasis is mediated by brassinosteroid feedback signaling. *Curr Biol* 22(18):1732–7.
24. Robatzek S, et al. (2006) Ligand-induced endocytosis of the pattern recognition receptor FLS2 in Arabidopsis service Ligand-induced endocytosis of the pattern recognition receptor FLS2 in Arabidopsis. 537–542.
25. Kohorn BD, Kohorn SL (2012) The cell wall-associated kinases, WAKs, as pectin receptors. *Front Plant Sci* 3(May):88.
26. Wang L, et al. (2015) Spatiotemporal Dynamics of the BRI1 Receptor and its Regulation by Membrane Microdomains in Living Arabidopsis Cells. (September):1334–1349.
27. Zhou J, et al. (2018) Regulation of *Arabidopsis* brassinosteroid receptor BRI1 endocytosis and degradation by plant U-box PUB12/PUB13-mediated ubiquitination. *Proc Natl Acad Sci*:201712251.
28. Hutten SJ, et al. (2017) Visualization of BRI1 and SERK3/BAK1 Nanoclusters in Arabidopsis Roots. *PLoS One* 12(1):e0169905.
29. Koller T, Bent AF (2014) FLS2-BAK1 Extracellular Domain Interaction Sites Required for Defense Signaling Activation. *PLoS One* 9(10):e111185.
30. Liu Y, Fire AZ, Boyd S, Olshen RA (2014) Estimating Clonality. *Genome Biol* 10(12):1–11.
31. Rubin-Delanchy P, et al. (2015) Bayesian cluster identification in single-molecule localization microscopy data. *Nat Meth* 12(11):1072–1076.
32. Saka SK, et al. (2014) Multi-protein assemblies underlie the mesoscale organization of the plasma membrane. *Nat Commun* 5(May):4509.
33. Hosy E, Martinière A, Choquet D, Maurel C, Luu D-T (2015) Super-Resolved and Dynamic Imaging of Membrane Proteins in Plant Cells Reveal Contrasting Kinetic Profiles and Multiple Confinement Mechanisms. *Mol Plant* 8(2):339–342.
34. Szymanski WG, et al. (2015) Cytoskeletal Components Define Protein Location to Membrane Microdomains. *Mol Cell Proteomics* 14(9):2493–2509.
35. Machta BB, Papanikolaou S, Sethna JP, Veatch SL (2011) Minimal model of plasma membrane heterogeneity requires coupling cortical actin to criticality. *Biophys J* 100(7):1668–1677.
36. Denness L, et al. (2011) Cell wall damage-induced lignin biosynthesis is regulated by a reactive oxygen species- and jasmonic acid-dependent process in Arabidopsis. *Plant Physiol* 156(3):1364–74.
37. Frischknecht R, et al. (2009) Brain extracellular matrix affects AMPA receptor lateral mobility and short-term synaptic plasticity. *Nat Neurosci* 12(7):897–904.
38. Ali GS, Prasad KVSK, Day I, Reddy ASN (2007) Ligand-dependent reduction in the

membrane mobility of Flagellin sensitive2, an Arabidopsis receptor-like kinase. *Plant Cell Physiol* 48(11):1601–1611.

39. Li X, et al. (2011) Single-Molecule Analysis of PIP2;1 Dynamics and Partitioning Reveals Multiple Modes of Arabidopsis Plasma Membrane Aquaporin Regulation. *Plant Cell* 23(10):3780–3797.

40. Boursiac Y, et al. (2005) Early Effects of Salinity on Water Transport in Arabidopsis Roots . Molecular and Cellular Features of Aquaporin Expression 1. 139(October):790–805.

41. Martinière A, et al. (2011) Homeostasis of plasma membrane viscosity in fluctuating temperatures. *New Phytol* 192(2):328–37.

42. Di Rubbo S, et al. (2013) The clathrin adaptor complex AP-2 mediates endocytosis of brassinosteroid insensitive1 in Arabidopsis. *Plant Cell* 25(8):2986–97.

43. Press WH, Teukolsky SA, Vetterling WT, Flannery BP (1992) *Numerical Recipes in C: The Art of Scientific Computing, Volume 1* (University of Cambridge).

44. Bruchle C, Lamb DC, Michaelis J eds. (2009) *Single Particle Tracking and Single Molecule Energy Transfer* (Wiley-VCH Verlag GmbH & Co. KGaA, Weinheim, Germany) doi:10.1002/9783527628360.

**Acknowledgements:**

JFM was funded by BBSRC grant BB/K009370/1 awarded to JR. AFT was funded by an Oxford Brookes Nigel Groome studentship. DR, SEDW, SB and MM are funded by the STFC. Access to the STFC funded facilities for TIRF-SP imaging was provided by programme access grant 16130041 to JR and CH. We thank T. Ott, S. Robatzek and J. Chan for generously providing seed lines. We would also like to thank all members of the plant cell biology section at Oxford Brookes for insightful discussions.

**<u>Figures</u>**

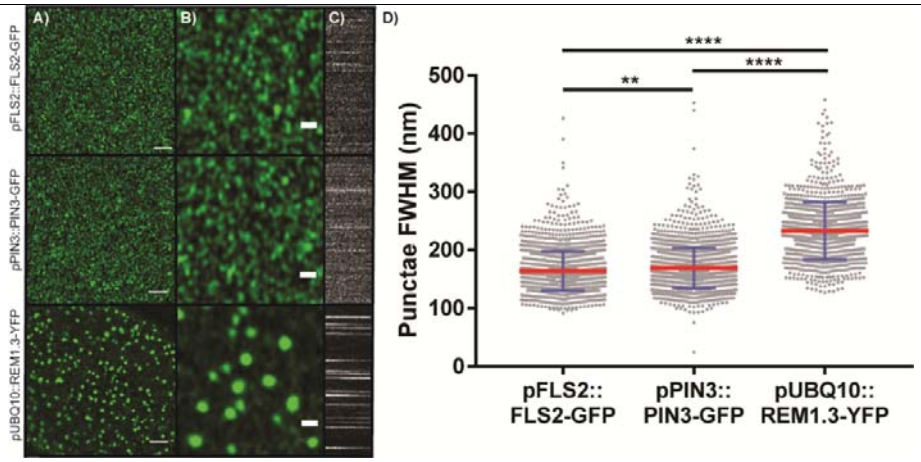


**Figure 1 PM proteins form clusters in the hypocotyl membrane**

A) Airyscan imaging of pFLS2::FLS2-GFP, pPIN3::PIN3-GFP and pUBQ10::REM1.3-YFP clusters in the membrane of stably-transformed *A. thaliana*, scale bar = 2µm. B) Digitally magnified image of those in A) showing clusters in more detail, scale bar= 500nm. C) Kymographs show dynamics of each nanocluster over time A) x = time, y = line profile. D) Box-and-whisker plot of full width half maximum (FWHM) measurement of cluster diameter for PM proteins in A). Nanodomain diameter differs significantly for each protein pair. **=P<0.01 and ****=P<0.0001, ANOVA with multiple comparisons.

575

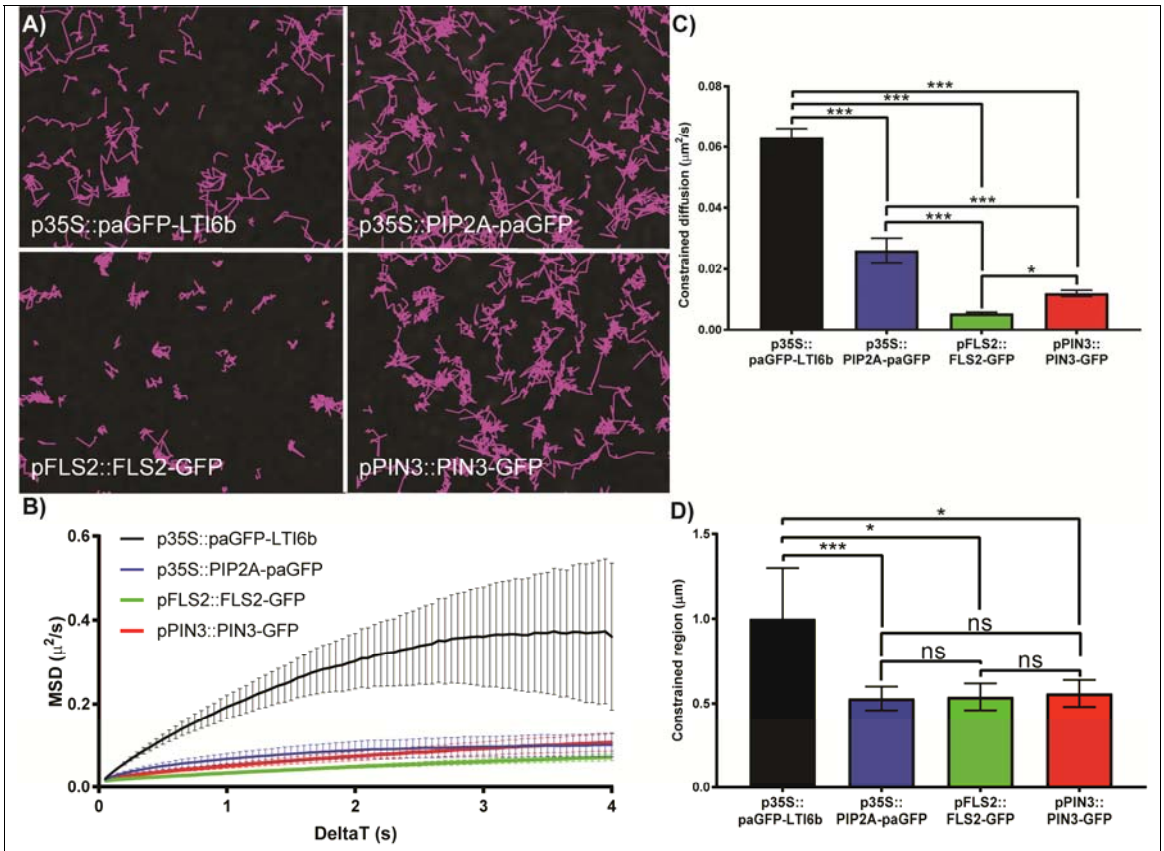


**Figure 2 TIRF single particle imaging of PM proteins**

A) TIRF single particle imaging of PM proteins in the hypocotyl membrane. Images show tracks followed by single labelled particles over 60s. Some proteins, e.g. FLS2-GFP are much more constrained in their lateral mobility than others. B) Mean Square Displacement curve for proteins. Curves that fall below a straight line corresponding to the initial gradient represent constrained diffusive movement. Error bars bootstrap-estimated standard deviation (see Methods). C) Constrained diffusion rate ($\mu m^2$/sec) of proteins in the membrane. All proteins tested differ. D) Constrained region area (µm) proteins occupy in the membrane. * = $p<0.05$, *** = $p<0.01$, ns = not significant.

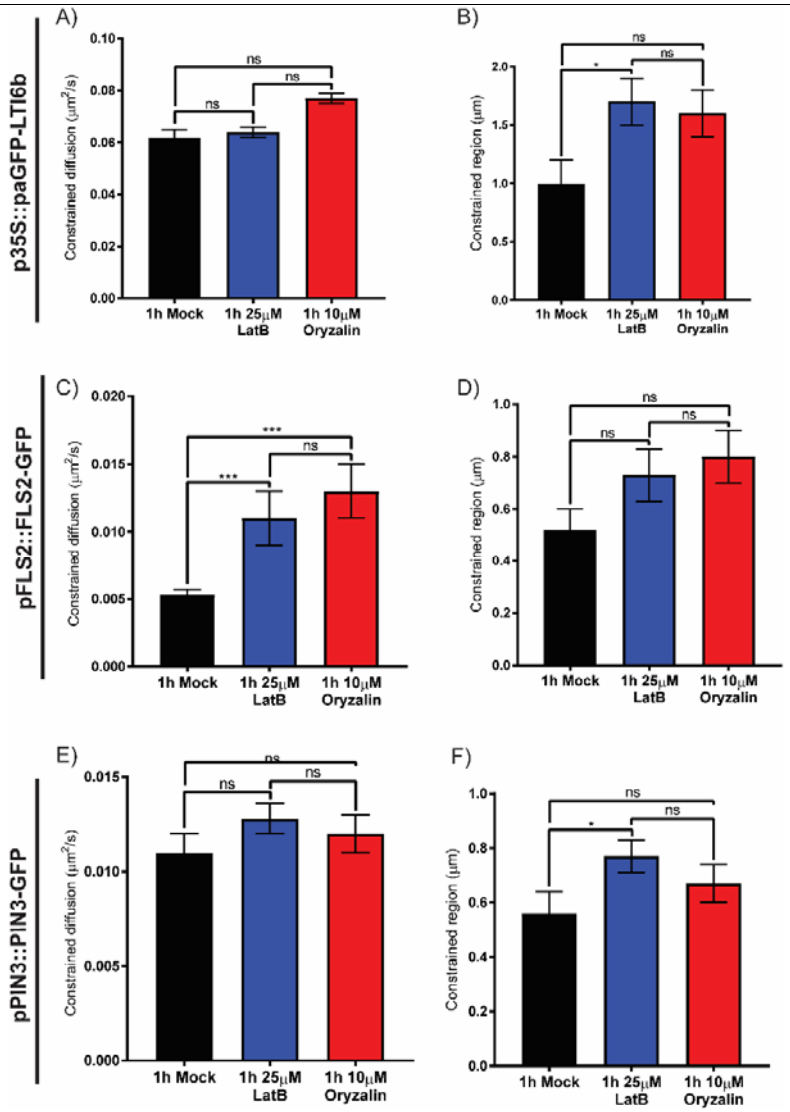


**Figure 3 Actin cytoskeleton regulates the mobility of FLS2-GFP in the membrane**

Plots show constrained diffusion rate (A, C, and E) and constrained area (B, D, and F) of single particles within the PM of hypocotyl epidermal cells in controls and after treatment with latrunculin B (LatB) and oryzalin to depolymerize the actin and microtubule cytoskeletons, respectively. A-B) p35S::paGFP-LTI6b, C-D) pFLS2::FLS2-GFP, and E-F) pPIN3::PIN3-GFP. FLS2-GFP becomes significantly more dynamic when either cytoskeleton is depolymerized. * = $p<0.05$, *** = $p<0.01$.

578

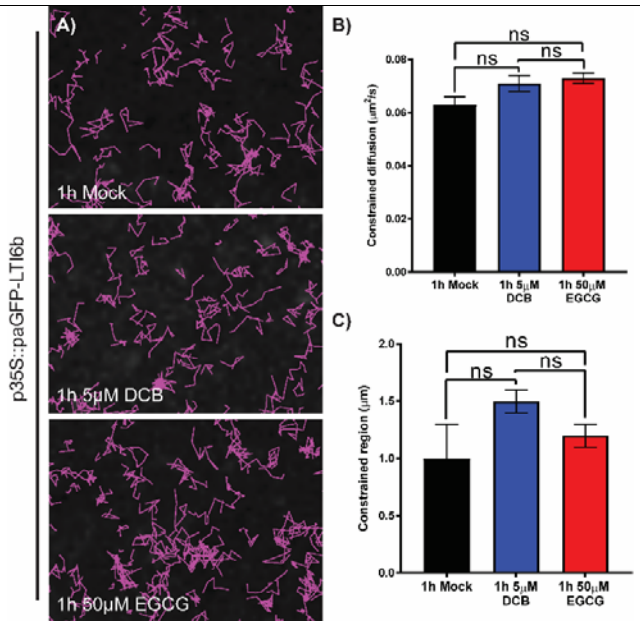


**Figure 4 Single particle tracking reveals little effect of cell wall perturbation on paGFP-LTI6b dynamics**

DCB was used to perturb cellulose synthesis and EGCG was used to perturb pectin methylation status of hypocotyl epidermal cells. A) p35S::paGFP-LTI6b in control, and after 5µM DCB and 50µM EGCG treatments for one hour each. Particles tracked over 60s. B) Constrained diffusion rate ($\mu m^2$/sec) of proteins in the membrane tracked over 4 seconds. C) Constrained region ($\mu m^2$) proteins occupy in the membrane during 4 seconds. ns = not significant.

579

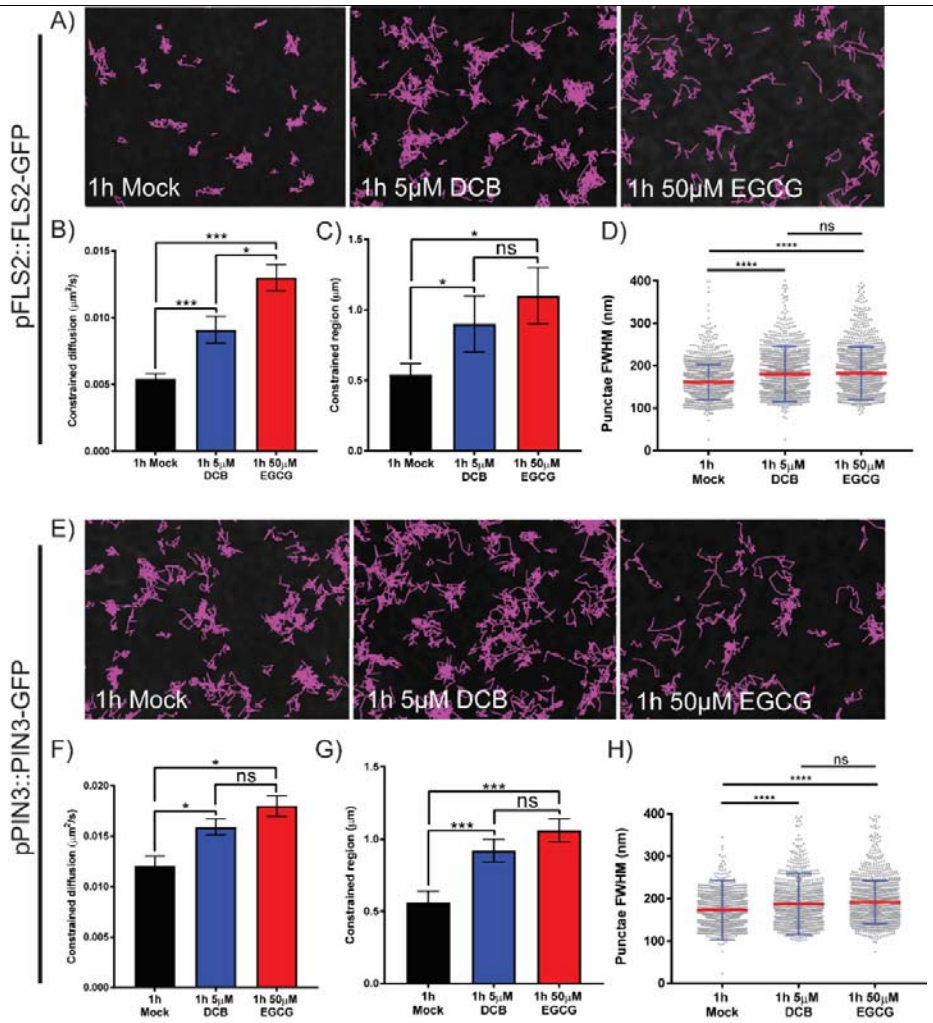


**Figure 5 Cell wall perturbation alters diffusion rate, constrained area and cluster size of FLS2-GFP and PIN3-GFP**

DCB was used to perturb cellulose synthesis and EGCG was used to perturb pectin methylation status of hypocotyl epidermal cells. A-D) Nanodomain characteristics of pFLS2::FLS2-GFP in either controls, or after treatment with 5μM DCB or 50μM EGCG for one hour. A) Track length of single particles over 60s. B) Constrained diffusion rate over 4s. C) Constrained region area over 4s. D) FWHM measurement of cluster diameter. Box-and-whiskers plots. E-H) Nanodomain characteristics of pPIN3::PIN3-GFP in either controls, or after treatment with 5μM DCB or 50μM EGCG for one hour. A) Track length of single particles over 60s. B) Constrained diffusion rate over 4s. C) Constrained region area over 4s. D) FWHM measurement of cluster diameter. Box-and-whiskers plots. There was a significant increase or trend towards increase in all nanodomain characteristics after cell wall pertebration. * = $p<0.05$, *** = $p<0.01$, ****=$p<0.001$.

**List of supplemental Materials**

1. **Supplementary Table 1** Number of tracks analysed per construct per treatment for single particle imaging
2. **Supplementary Table 2** Number of nanodomain puntae measured per construct per treatment for Airyscan imaging
3. **Supplemental Figure 1** Comparison of Confocal and Airyscan imaging of PM nanodomains
4. **Supplemental Figure 2** Instantaneous diffusion values for single particle tracking of PM proteins
5. **Supplemental Figure 3** Images and instantaneous diffusion values for p35S:: paGFP-LTI6b, pPIN3::PIN3-GFP and pFLS2::FLS2-GFP during cytoskeleton perturbation
6. **Supplemental Figure 4** Plasmolysis causes changes in single particle dynamics for LTI6b, FLS2 and PIN3
7. **Supplemental Figure 5** Instantaneous diffusion values for p35S::paGFP-LTI6b, pPIN3::PIN3-GFP and pFLS2::FLS2-GFP during cell wall perturbation
8. **Supplemental Movie 1** Single particle tracking of LTI6b, PIP2A, FLS2 and PIN3 shows they diffuse at different rates and occupy differing sized areas within the PM.
9. **Supplemental Movie 2** Single particle tracking of LTI6B, PIP2A, FLS2 and PIN3 during mock, actin (Lat-B) and microtubule (Oryzalin) depolymerisation
10. **Supplemental Movie 3** Single particle tracking of LTI6b in the PM during cell wall perturbation
11. **Supplemental Movie 4** Single particle tracking of LTI6b in the PM during plasmolysis
12. **Supplemental Movie 5** Single particle tracking of FLS2 and PIN3 during cell wall perturbation.
13. **Supplemental Movie 6** Single particle tracking of FLS2 and PIN3 during plasmolysis.